

The distance sum rule from strong lensing systems and quasars - test of cosmic curvature and beyond

Jing-Zhao Qi^{1,2}, Shuo Cao^{2,*}, Sixuan Zhang², Marek Biesiada^{2,3,†}, Yan Wu²
and Zong-Hong Zhu²

¹ Department of Physics, College of Sciences, Northeastern University, Shenyang 110819, China;

² Department of Astronomy, Beijing Normal University, Beijing 100875, China;

³ Department of Astrophysics and Cosmology, Institute of Physics, University of Silesia, 75 Pulku Piechoty 1, 41-500 Chorzów, Poland

Accepted XXX. Received YYY; in original form ZZZ

ABSTRACT

Testing the distance-sum-rule in strong lensing systems provides an interesting method to determine the curvature parameter Ω_k using more local objects. In this paper, we apply this method to a quite recent data set of strong lensing systems in combination with intermediate-luminosity quasars calibrated as standard rulers. In the framework of three types of lens models extensively used in strong lensing studies (SIS model, power-law spherical model, and extended power-law lens model), we show that the assumed lens model has a considerable impact on the cosmic curvature constraint, which is found to be compatible or marginally compatible with the flat case (depending on the lens model adopted). Analysis of low, intermediate and high-mass sub-samples defined according to the lens velocity dispersion demonstrates that, although it is not reasonable to characterize all lenses with a uniform model, such division has little impact on cosmic curvature inferred. Finally, thinking about future when massive surveys will provide their yields, we simulated a mock catalog of strong lensing systems expected to be seen by the LSST, together with a realistic catalog of quasars. We found that with about 16000 such systems, combined with the distance information provided by 500 compact milliarcsecond radio sources seen in future radio astronomical surveys, one would be able to constrain the cosmic curvature with an accuracy of $\Delta\Omega_k \simeq 10^{-3}$, which is comparable to the precision of *Planck* 2015 results.

Key words: cosmology: observations – cosmology: miscellaneous

1 INTRODUCTION

Since the beginning of modern cosmology, the curvature parameter Ω_k of the Universe has been one of the most important cosmological parameters one attempted to measure. Its value, or even its sign, bears important information on the matter-energy budget in the Universe and sheds light on its ultimate fate. Moreover, it clarifies which one of three possible classes of Friedman-Lemaître-Robertson-Walker (FLRW) metric correctly describes our Universe and is adequate for cosmological inference. New, precise measurements of anisotropies in the cosmic microwave background radiation (CMBR) convinced us that the Universe we live in is spatially flat as it was expected by the supporters of inflationary models. The latest, most precise constraint, $|\Omega_k| < 0.005$, comes from the *Planck* satellite's

CMBR data (Ade et al. 2016). Such constraints are possible since the acoustic horizon scale, corresponding to the distance that sound waves could have traveled between the birth of the universe and the time when the CMBR was emitted (the surface of last scattering) can be calculated theoretically. So it can be used as a standard ruler imprinted in the CMBR anisotropy patterns. Its apparent size depends on whether the Universe is flat, negatively or positively curved, which underlies the measurement of curvature parameter from CMBR anisotropies. The length of this standard ruler is somewhat degenerate with quantities such as the matter density or dark energy equation of state. Therefore, cosmic curvature inferred from CMBR is model-dependent to some extent (Ade et al. 2016).

New dimension to the significance of cosmic curvature measurements has been given by the works of Clarkson et al. (2008); Räsänen et al. (2015). They realized that measurements of the cosmic curvature using extragalactic objects

* E-mail: caoshuo@bnu.edu.cn

† E-mail: marek.biesiada@us.edu.pl

(standard rulers and standard candles detected in future all-sky surveys) could serve as a test of the Copernican Principle i.e. the validity of the FLRW metric. Moreover, [Bolejko \(2017b,a\)](#) examined the emergence of negative spatial curvature within the so called silent universe in which the back-reaction of inhomogeneities (coming from the structure formation) was taken into account. This effect could potentially be detected using closer objects instead of CMBR. Measurements of Ω_k according to the idea of [Clarkson et al. \(2008\)](#) have been performed using the current observational data comprising supernovae Ia (SN Ia) (standard candles) and Hubble parameters $H(z)$ inferred from cosmic chronometers ([Cai et al. 2016](#); [Li et al. 2016c](#); [Wei & Wu 2017](#); [Rana et al. 2017](#)) (see [Qi et al. \(2018\)](#) for the latest measurements of $H(z)$ data). It was found that the cosmic curvature estimated this way is well consistent with the flat case of $\Omega_k = 0$. One should mention that also other methods to measure the cosmic curvature have been discussed. [Takada & Doré \(2015\)](#) proposed that combined radial and angular diameter distances from the BAO can be used to constrain the curvature parameter. The achievable accuracy of such Ω_k measurement could be $\Delta\Omega_k \simeq 10^{-3}$. [Denissenya et al. \(2018\)](#) used the measurements of strong lensing time delays and supernova distance to measure the curvature. In other papers, measurements of Ω_k are discussed using the mean image separation statistics of gravitationally lensed quasars ([Rana et al. 2017](#)) or in the non-flat Λ CDM inflation model ([Ooba et al. 2018](#)).

The approach of [Räsänen et al. \(2015\)](#) involves strong gravitational lensing (SGL) systems, where three objects in the Universe (the source, the lens and the observer) are almost perfectly aligned. This setting allows testing the type of FLRW metric (and thus Ω_k) using the distance sum rule ([Liao et al. 2017](#)). More recently, this method has been applied by [Xia et al. \(2017\)](#) on a SGL sample including 118 galactic-scale systems compiled by [Cao et al. \(2015b\)](#). In all these previous works, distances were inferred from type Ia supernova (SN Ia) acting as standard candles. However, as discussed in the literature ([Wei & Wu 2017](#); [Li et al. 2016c](#)), using SN Ia data generates considerable uncertainty of derived Ω_k , due to several nuisance parameters characterizing the SN light-curves. Moreover, the limited redshift range of SN Ia, i.e. $z \leq 1.40$ implies that only a limited number of known SGL systems can be used, and higher redshift SGL systems cannot be matched with SN Ia ([Xia et al. 2017](#)). Finally, the use of SN Ia data in this context relies on the so-called Etherington duality principle connecting luminosity and angular diameter distances. This distance duality is valid in any metric theory. However, it relies on the assumption that photons are conserved along the path from the source to observer, which potentially might be violated ([Holanda et al. 2011](#); [Cao & Zhu 2011](#); [Cao & Liang 2011](#); [Cao & Zhu 2014](#)).

It is clear that, for the purpose of implementing the method of [Räsänen et al. \(2015\)](#), it would be beneficial to use distance probes covering higher redshifts thus taking advantage of larger sample of SGL systems. In this paper we use the latest catalog of strong gravitational lensing systems ([Cao et al. 2015b](#)) to extract the distance ratio $\frac{d_{ls}}{d_s}$. Moreover, for the purpose of distance estimation we use the recently compiled sample of milliarcsecond compact radio-sources data set comprising 120 intermediate-

luminosity quasars calibrated as standard rulers and covering the redshift range $0.46 < z < 2.76$ ([Cao et al. 2017b](#)). This paper is organized as follows: In section 2 we describe the methodology and the data used in our work. We discuss our results in section 3. Section 4 demonstrates the performance of our method on simulated yields of future surveys. Finally, the conclusions are presented in section 5.

2 METHODOLOGY AND DATA

We assume that in the homogeneous and isotropic universe, its geometry can be described by the FLRW metric

$$ds^2 = -dt^2 + \frac{a(t)^2}{1 - kr^2} dr^2 + a(t)^2 r^2 d\Omega^2, \quad (1)$$

where k represents the spatial curvature. $k = +1, -1, 0$ corresponds to closed, open, and flat universe, respectively and is related to the curvature parameter as $\Omega_k = -k/H_0^2$.

For a given strong lensing system with the source at redshift z_s and lensing galaxy at redshift z_l the separation of multiple images depends on the ratio $D_A(z_l, z_s)/D_A(z_s)$ of angular-diameter distances between the lens and the source and between the observer and the source, provided one has a reliable model for the mass distribution of the lens ([Grillo et al. 2008](#); [Biesiada et al. 2010](#); [Cao et al. 2012, 2015b](#)). The dimensionless distance $d(z)$ between the lensing galaxy and the source is given by

$$\begin{aligned} d(z_l, z_s) &= (1 + z_s)H_0 D_A(z_l, z_s) \\ &= \frac{1}{\sqrt{|\Omega_k|}} \begin{cases} \sinh \sqrt{|\Omega_k|} \int_{z_l}^{z_s} \frac{H_0 dz'}{H(z')}, & k < 0, \\ \sqrt{|\Omega_k|} \int_{z_l}^{z_s} \frac{H_0 dz'}{H(z')}, & k = 0, \\ \sin \sqrt{|\Omega_k|} \int_{z_l}^{z_s} \frac{H_0 dz'}{H(z')}, & k > 0, \end{cases} \end{aligned} \quad (2)$$

where $\Omega_k = -k/H_0^2$. For convenience, we denote $d_{ls} \equiv d(z_l, z_s)$, $d_l \equiv d(0, z_l)$ and $d_s \equiv d(0, z_s)$. According to the distance sum rule ([Räsänen et al. 2015](#)), these three dimensionless distances satisfy the following relation

$$\frac{d_{ls}}{d_s} = \sqrt{1 + \Omega_k d_l^2} - \frac{d_l}{d_s} \sqrt{1 + \Omega_k d_s^2}. \quad (3)$$

Therefore, if the distances d_l , d_s and d_{ls} are obtained from observations, the value of Ω_k could be directly derived without the involvement of any specific cosmological model. In this paper, the distance ratio d_{ls}/d_s is extracted from SGL systems, while the other two distances, d_l and d_s , are obtained through the angular size measurements of compact structure in radio quasars calibrated as standard rulers.

2.1 Strong gravitational lensing systems

Since the discovery of the first gravitational lens Q0957+561 ([Walsh et al. 1979](#)), and with the increasing size of SGL systems detected strong lensing has become a serious and important technique in extragalactic astronomy (exploration of galactic structure) ([Ofek et al. 2003](#); [Cao et al. 2016](#)) and in cosmology ([Biesiada et al. 2010, 2011](#); [Cao & Liang 2011](#); [Cao & Zhu 2012](#); [Cao et al. 2012, 2015b](#); [Li et al. 2016a](#)). Since early-type galaxies are more massive and dominate in all strong lensing surveys, we will consider only SGL systems in which elliptical galaxies act as lenses. Although the properties of early-type galaxies, their formation and evolution

are still not fully understood in details, singular isothermal sphere (SIS) and singular isothermal ellipsoid (SIE) models are commonly used to describe the mass distribution of lensing galaxies acting as lenses (Koopmans et al. 2006).

We will consider three types of lens models which have been extensively used in strong lensing studies.

i) SIS model: Assuming that the elliptical galaxy modeled as singular isothermal sphere (SIS) acts as a lens, the distance ratio can be expressed as

$$\frac{d_{ls}}{d_s} = \frac{c^2 \theta_E}{4\pi \sigma_{SIS}^2} \quad (4)$$

The velocity dispersion σ_{SIS} reflects the total mass of the lens (including dark matter). In order to quantify its relation to the observed velocity dispersion of stars σ_0 , we introduce a free parameter $f_E = \sigma_{SIS}/\sigma_0$ with the corresponding prior of $0.8 < f_E^2 < 1.2$ (Ofek et al. 2003; Cao et al. 2012).

ii) Power-law spherical model: We assume that the total mass density profile follows spherically symmetric power-law distribution $\rho \sim r^{-\gamma}$, where r is the spherical radius from the center of the lensing galaxy. Combined with the spherical Jeans equation, one can express observational value of the angular-diameter distance ratio as (Koopmans et al. 2006; Cao et al. 2015b)

$$\frac{d_{ls}}{d_s} = \frac{c^2 \theta_E}{4\pi \sigma_{ap}^2} \left(\frac{\theta_{ap}}{\theta_E} \right)^{2-\gamma} f^{-1}(\gamma), \quad (5)$$

where

$$f(\gamma) = -\frac{1}{\sqrt{\pi}} \frac{(5-2\gamma)(1-\gamma)}{3-\gamma} \frac{\Gamma(\gamma-1)}{\Gamma(\gamma-3/2)} \left[\frac{\Gamma(\gamma/2-1/2)}{\Gamma(\gamma/2)} \right]^2. \quad (6)$$

Note that σ_{ap} is the velocity dispersion of the lens obtained inside an aperture radius θ_{ap} (more precisely, luminosity-averaged line-of-sight velocity dispersion). Moreover, we allow the power-law index to vary with redshift $\gamma(z) = \gamma_0 + \gamma_1 z$ in order to account for the possible evolution of the mass density profile. The analysis performed by Ruff et al. (2011) using the same parametrization of $\gamma(z)$ revealed the following results: $\gamma(z_l) = 2.12^{+0.03}_{-0.04} - 0.25^{+0.10}_{-0.12} \times z_l + 0.17^{+0.02}_{-0.02}$, where the last term denotes the Gaussian scatter about that linear relation. Similar works aimed at establishing the evolution of mass density profile with different samples of lens galaxies have also been attempted in the literature (Koopmans et al. 2006; Bolton et al. 2012). In our analysis, γ_0 and γ_1 are treated as free parameters together with cosmological ones.

iii) Extended power-law model: As a third lens model we consider a more complex one, which allows the luminosity density profile $\nu(r)$ differ from the total-mass density profile $\rho(r)$, both of them modeled by corresponding power-laws $\rho \sim r^{-\alpha}$, $\nu \sim r^{-\delta}$. Moreover, we consider the anisotropic distribution of three-dimensional velocity dispersion, i.e. we admit that radial and tangential velocity dispersions might be different. This is captured in the anisotropy parameter: $\beta(r) = 1 - \sigma_t^2/\sigma_r^2$. In this model the observational value of the distance ratio is given by (Schwab et al. 2009)

$$\begin{aligned} \frac{d_{ls}}{d_s} &= \left(\frac{c^2}{4\sigma_0^2} \theta_E \right) \frac{2}{\sqrt{\pi}(\xi-2\beta)} \left(\frac{\theta_{ap}}{\theta_E} \right)^{2-\alpha} \\ &\times \left[\frac{\lambda(\xi) - \beta\lambda(\xi+2)}{\lambda(\alpha)\lambda(\delta)} \right] \frac{\Gamma(\frac{3-\xi}{2})}{\Gamma(\frac{3-\delta}{2})}, \end{aligned} \quad (7)$$

where $\xi = \alpha + \delta - 2$, and $\lambda(x) = \Gamma(\frac{x-1}{2})/\Gamma(\frac{x}{2})$. Following the analysis of Cao et al. (2015b), we will model the anisotropy parameter by a Gaussian distribution $\beta = 0.18 \pm 0.13$, based on the well-studied sample of nearby elliptical galaxies.

The methodology described above is implemented to the sample of 118 galactic scale SGL systems from the Sloan Lens ACS Survey (SLACS), BOSS emission-line lens survey (BELLS), Lens Structure and Dynamics (LSD) and Strong Lensing Legacy Survey (SL2S) assembled by Cao et al. (2015b). Moreover, recent analysis of different sub-samples lenses defined according to their redshifts and velocity dispersions (i.e. effectively according to their masses) showed that it is necessary to investigate separately low-, intermediate- and high-mass galaxies (Cao et al. 2016). Since the redshift range covered by lenses was not large enough to display any noticeable differences, the division according to velocity dispersion turned out to be more discriminative. Therefore, we also divide the SGL sample into three sub-samples based on lens velocity dispersion: $\sigma_{ap} \leq 200 \text{ km s}^{-1}$ (low-mass galaxies), $200 \text{ km s}^{-1} < \sigma_{ap} \leq 300 \text{ km s}^{-1}$ (intermediate-mass galaxies) and $\sigma_{ap} > 300 \text{ km s}^{-1}$ (high-mass galaxies), and study the effect on the measurement of curvature caused by such division.

2.2 Radio quasar data

Currently, the possibility of using compact radio sources to study cosmological parameters and physical properties of AGNs became very attractive in the literature (Jackson & Dodgson 1997; Vishwakarma 2001; Lima & Alcaniz 2002; Zhu & Fujimoto 2002; Chen & Ratra 2003). More interestingly, the advantage of radio quasars, compared with other standard rulers including baryon acoustic oscillations (BAO) (Percival et al. 2010), galaxy clusters (Bonamente et al. 2006), and strong lensing systems (Cao et al. 2012, 2015b), lies in the fact that is that quasars are observed at much higher redshifts. Our procedure follows the phenomenological model originally proposed in Gurvits (1994) and later investigated in Gurvits et al. (1998), which quantifies the luminosity and redshift dependence of the linear sizes of quasars as

$$l_m = lL^\beta (1+z)^n, \quad (8)$$

where β and n are two constant parameters quantifying the ‘‘angular size-luminosity’’ and ‘‘angular size-redshift’’ relations. Therefore, constraints on β and n will help us to differentiate between sub-samples. In particular the sub-sample of compact radio sources fulfilling $\beta = n = 0$ could act as standard rulers. Considering the VLBI visibility data for 337 active galactic nuclei (AGN), Gurvits (1994) provided a rough estimation of the dependence of apparent angular sizes on the luminosity and redshifts: $\beta \sim 0.26$, and $n \sim -0.30$, under assumption of homogeneous and isotropic universe without cosmological constant. Regression analysis of the restricted sample with spectral index ($-0.38 \leq \alpha \leq 0.18$) and total luminosity ($Lh^2 \geq 10^{26} \text{ W/Hz}$), gave a value of $\beta \sim 0.37$ and $n \sim -0.58$ (Gurvits et al. 1998). Following this direction, in the framework of concordance Λ CDM cosmology Cao et al. (2015a) in attempt to determine intrinsic linear sizes of compact structure in 112 radio quasars found a substantial evolution of linear

sizes with luminosity ($\beta \sim 0.17$) and much smaller cosmological evolution of the linear size ($|n| \simeq 10^{-2}$). More recently, the use of intermediate-luminosity quasars (10^{27} W/Hz $< L < 10^{28}$ W/Hz) as potential cosmological tracers was studied in detail in [Cao et al. \(2017a\)](#). The sample of 613 milliarcsecond ultra-compact radio sources based on a 2.29 GHz VLBI all-sky survey ([Kellermann 1993](#); [Gurvits 1994](#)), was divided into different sub-samples, according to their optical counterparts and luminosity: low, intermediate, and high-luminosity quasars. Luminosity selection as well as $D_A(z)$ assessments necessary for building the sample were performed without pre-assuming a cosmological model but basing on the $D_A(z)$ reconstruction from $H(z)$ data obtained from cosmic chronometers ([Jimenez & Loeb 2002](#); [Moresco et al. 2012](#)). Further detailed analysis revealed that only intermediate-luminosity quasars (ILQSO) show negligible dependence on both redshifts z and intrinsic luminosity L ($|n| \simeq 10^{-3}$, $\beta \simeq 10^{-4}$), which makes them a fixed comoving-length standard ruler. Subsequently, [Cao et al. \(2017b\)](#) used an improved cosmological-model-independent method to calibrate the linear sizes of ILQSO as $l_m = 11.03 \pm 0.25$ pc at 2.29 GHz. Cosmological application of this data set ([Cao et al. 2017b](#)) resulted with stringent constraints on both the matter density parameter Ω_m and the Hubble constant H_0 , in a very good agreement with recent *Planck* 2015 results ([Ade et al. 2016](#)). The exploration of other cosmological models in light of this observational data has been broadly studied in the literature ([Li et al. 2017](#); [Qi et al. 2017](#); [Ma et al. 2017](#); [Zheng et al. 2017](#); [Xu et al. 2018](#); [Cao et al. 2018](#)). In the context of our study, it is reasonable to ask whether uncertainties in the standard ruler assumption generate additional systematic errors on the final result. In order to address this issue, we performed a sensitivity analysis by applying Monte Carlo simulations in which β , n parameters are characterized by Gaussian distributions: $\beta = 0.00 \pm 0.05$ and $n = 0.00 \pm 0.05$, respectively, while the uncertainty of the linear size scaling factor was taken into account with a Gaussian distribution as $l = 11.03 \pm 0.25$ pc. In result the effects of uncertainties of l , β and n turned out to be negligible, especially for the reconstruction of $d(z)$ function from the quasar data.

We will use the above mentioned calibrated value of the linear size l_m to calculate the angular diameter distances to ILQSO sample ([Cao et al. 2017b](#))

$$D_A(z) = \frac{l_m}{\theta(z)}. \quad (9)$$

Then one can use angular diameter distances to the quasars to obtain the dimensionless distances to the lenses d_l and to the sources d_s (for each SGL system), as

$$d_l = \frac{H_0}{c}(1+z_l)D_A(z_l); \quad d_s = \frac{H_0}{c}(1+z_s)D_A(z_s). \quad (10)$$

For this purpose we assume the value of the Hubble constant $H_0 = 67.8 \text{ kms}^{-1}\text{Mpc}^{-1}$ after *Planck* Collaboration XIII (2015).

The problem is that in order to use ILQSO distances in Eq. (3) one should identify intermediate luminosity quasars at redshifts equal to (or at least very close to) the redshifts of sources and lenses in SGL systems from which distance ratio is inferred. This is not possible, but fortunately, a model-independent method of Gaussian processes (GP)

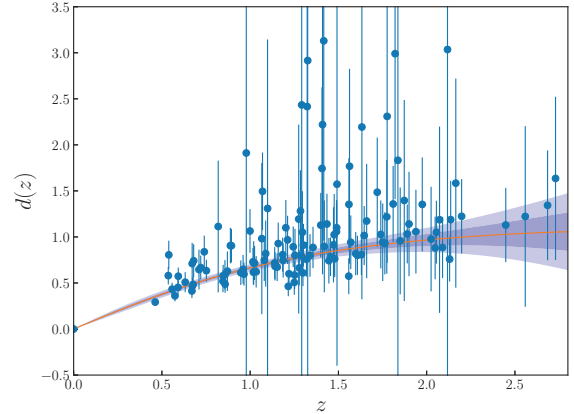


Figure 1. Reconstruction of $d(z)$ from the quasar sample. Shaded areas represent 68% and 95% confidence level of the reconstruction.

([Seikel et al. 2012a](#)), can be employed to reconstruct the dimensionless comoving distance from the data straightforwardly, without any parametric assumption regarding cosmological model. In this process, the values of the reconstructed function evaluated at any two different points z and \tilde{z} , are connected by a covariance function $k(z, \tilde{z})$. In this paper, we take the squared exponential form for covariance function $k(z, \tilde{z})$, which depends only on two hyper parameters σ_f and ℓ

$$k(z, \tilde{z}) = \sigma_f^2 \exp\left(-\frac{(z - \tilde{z})^2}{2\ell^2}\right). \quad (11)$$

The values of these hyper parameters can be optimized by the GP itself via the observed data. The GP approach has been used in various studies ([Seikel et al. 2012b](#); [Yang et al. 2015](#); [Li et al. 2016b](#); [Qi et al. 2016](#); [Zhang & Xia 2016](#)). Therefore, we use GP to reconstruct the profile of $d(z)$ from the quasar sample as shown in Fig. 1. Obviously, the anchoring point $d(0) = 0$ makes the uncertainty of the reconstructed $d(z)$ smaller at low redshifts. This reconstruction can be done up to the redshift $z = 2.8$. Considering the redshift range of lenses $0.075 \leq z_l \leq 1.004$ and sources $0.196 \leq z_s \leq 3.595$ in the original sample of 118 strong lenses, SGL systems with $z_s > 2.8$ should be excluded. This selection leaves us with 106 SGL systems and we performed our study on this sample, in which low-mass lensing galaxies contribute 20 data points ($0.075 \leq z_l \leq 0.682$), intermediate-mass galaxies contribute 73 data points ($0.082 \leq z_l \leq 0.938$), and high-mass galaxies contribute 13 data points ($0.164 \leq z_l \leq 1.004$).

Fig. 2 shows the redshift coverage of strong lensing systems, SN Ia and ILQSO. Compared with the previous works using the luminosity distances $D_L(z)$ of SN Ia ([Xia et al. 2017](#)), one can see that the intermediate luminosity quasars have better coverage of redshifts corresponding to the sources in SGL systems.

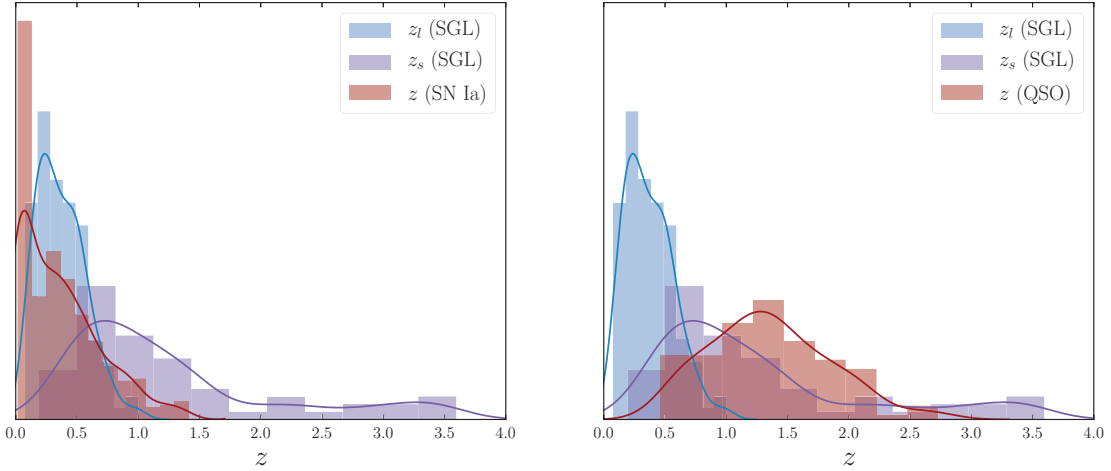


Figure 2. Redshift distribution of SGL systems and different cosmological probes used to assess distances. One can see that QSO sample has more fair coverage of the redshift range of SGL sources than SN Ia.

3 RESULTS AND DISCUSSIONS

The Ω_k parameter was determined by maximizing the likelihood $\mathcal{L} \sim \exp(-\chi^2/2)$ where the chi-square function was defined as:

$$\chi^2(\mathbf{p}, \Omega_k) = \sum_{i=1}^{106} \frac{(D_{th}(z_i; \Omega_k) - D_{obs}(z_i; \mathbf{p}))^2}{\sigma_D(z_i)^2}, \quad (12)$$

where $D = d_{ls}/d_s$ and its theoretical value (dependent on Ω_k) is given by the distance sum rule Eq. (3) and its observational counterpart is Eq. (4), Eq. (5) or Eq. (7) depending on the lens model adopted. Parameters of the lens model are denoted as \mathbf{p} . We fit both Ω_k and nuisance parameters \mathbf{p} and later we marginalize over the latter. Maximization was performed using the emcee Python module (Foreman-Mackey et al. 2013) based a Markov chain Monte Carlo (MCMC) code. Two factors contribute to the uncertainty of D : uncertainty from SGL systems and uncertainty from the distances reconstructed from ILQSO. We assume that being uncorrelated they add in quadrature: $\sigma_D^2 = \sigma_{SGL}^2 + \sigma_{QSO}^2$. Term from SGL systems comes from the uncertainty of velocity dispersion measurements (reported in the data set) and from the Einstein radius determination which we assume at the level of 5%. Exact formulae for these uncertainties in the lens models considered can be found in Cao et al. (2012, 2015b, 2016) respectively. Part of the uncertainty coming from quasars σ_{QSO} is determined as a width of the uncertainty strip of GP-reconstructed distance for a given redshift $z_{(l,s),i}$.

3.1 SIS model

Working on the SIS lens model, we obtained the results displayed in Fig. 3 and Table 1. The most stringent constraint on the cosmic curvature Ω_k was obtained from the full sample of SGL systems. Low and intermediate-mass lenses gave less stringent constraints. However, the flat Universe is supported in all these cases. Due to the limited sample size, high-mass sample was too small to give reasonable constraint. Concerning the f_E parameter, its best-

fitted value is different across the sub-samples. However, high and intermediate-mass lens samples agree with each other and with the full sample in the sense that their 1σ regions overlap. Low-mass sample differs from the rest up to 2σ interval. More interestingly, we find the SIS model ($f_E = 1$) is well consistent with results obtained in low-mass and intermediate-mass (low and intermediate velocity dispersion) galaxies. Consequently, our results imply that consideration of sub-samples defined according to velocity dispersions is necessary in SGL analysis.

3.2 Power-law spherical model

In the case of spherically symmetric power-law lens model (allowing for the evolution of the power-law exponent) we obtained the results shown in Fig. 4 and Table 2. For the full sample, the central fits are $\Omega_k < -0.0327$, $\gamma_0 = 2.054 \pm 0.064$ and $\gamma_1 = -0.20 \pm 0.26$. Marginalized distribution of Ω_k implies that, flat Universe is still compatible with the data within 2σ confidence interval. However, a closed universe seems to be more favored, which is also in good agreement with the results of previous works (Räsänen et al. 2015; Xia et al. 2017). It is, however, different from clearly preferred by the CMBR experiments (Ade et al. 2016). Even though our constraint on the cosmic curvature is not improved over the previous works (Räsänen et al. 2015; Xia et al. 2017), yet our approach more fairly covers the redshift range of sources whose angular diameter distances are being used. Let us stress again, that we have not only constrained the cosmic curvature, but also the evolution of slope factor in the mass density profile of lensing galaxies. Our results suggest that the total density profile of early-type galaxies have become slightly shallower over cosmic time, but it is still consistent with the standard SIS model ($\gamma_0 = 2$, $\gamma_1 = 0$) within 1σ uncertainty.

The analysis performed on sub-samples defined by the lens velocity dispersion reveals that, even though the best fitted values of slope parameters (γ_0 , γ_1) are different, they are all consistent with each other and with the full sample within 1σ regions. We note that the ranges of γ parameters, which

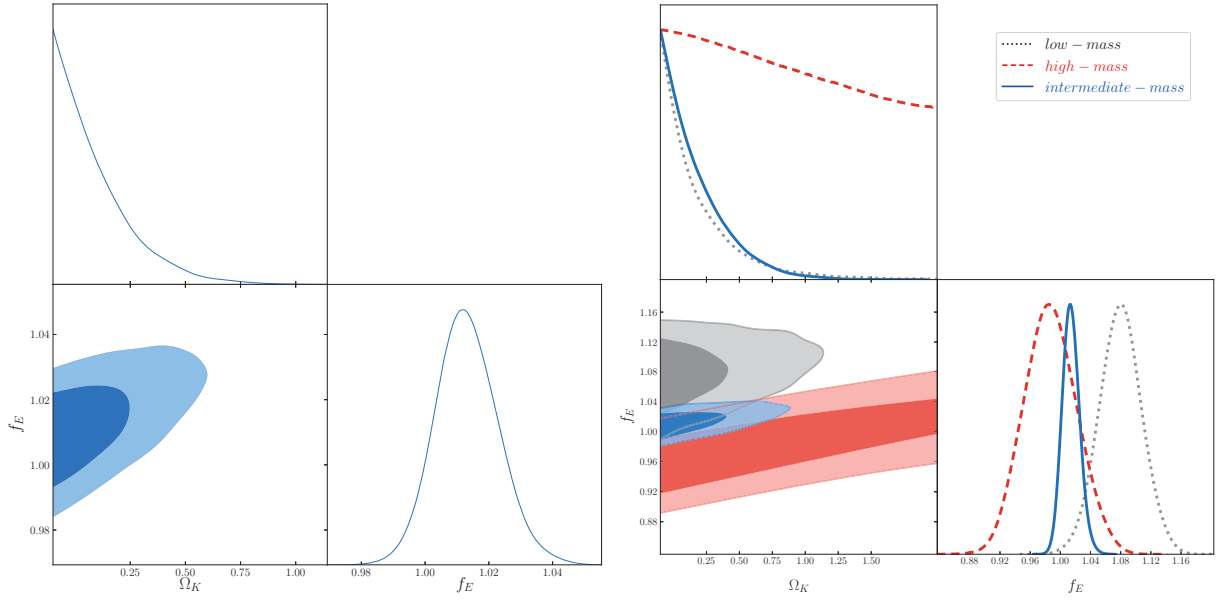


Figure 3. Left: 2-D distributions of cosmic curvature Ω_k and SGL parameters (f_E) constrained from the 106 SGL sample in the case of SIS lens model. 1σ and 2σ uncertainty contours are shown together with 1-D distributions of respective parameters marginalized over the remaining ones. Right: The results obtained from three sub-samples of SGL systems selected according to their velocity dispersions.

	low-mass	intermediate-mass	high-mass	full sample
Ω_k	< 0.231	< 0.227	—	< 0.136
f_E	1.08 ± 0.028	1.014 ± 0.011	0.987 ± 0.035	$1.0132^{+0.0092}_{-0.010}$

Table 1. Results from the SIS model: the best-fitted values of Ω_k and f_E with 68% confidence level for different samples.

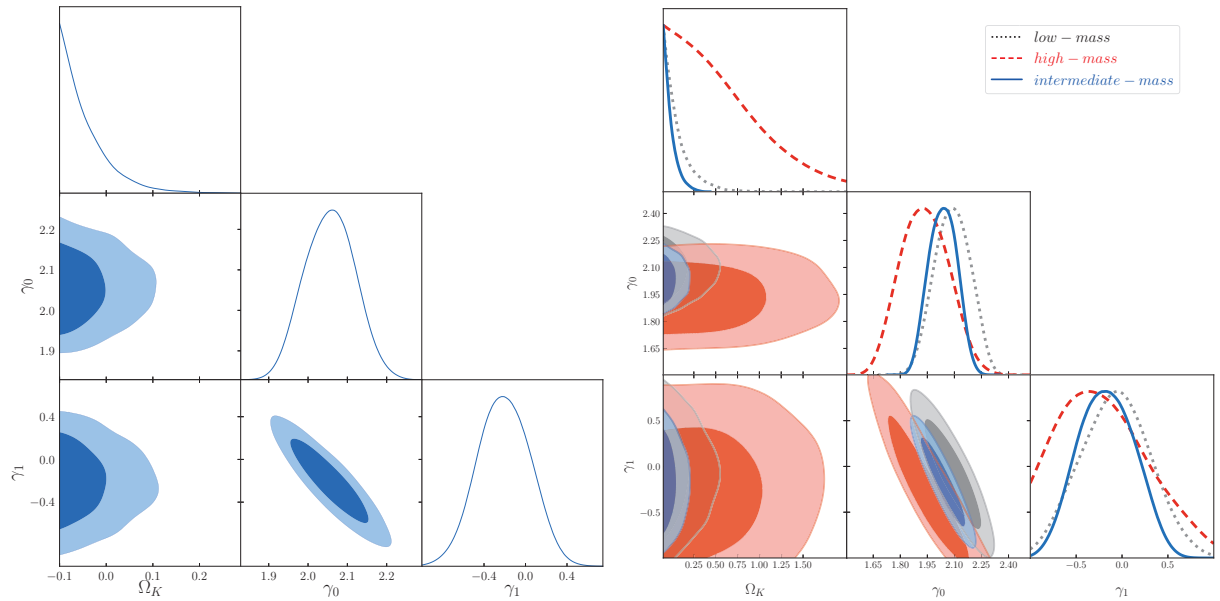


Figure 4. Left: 2-D distributions of cosmic curvature Ω_k and SGL parameters (γ_0 , γ_1) constrained from the 106 SGL sample in the case of spherically symmetric power-law lens model. 1σ and 2σ uncertainty contours are shown together with 1-D distributions of respective parameters marginalized over the remaining ones. Right: The results obtained from three sub-samples of SGL systems selected according to their velocity dispersions.

	low-mass	intermediate-mass	high-mass	full sample
Ω_k	< 0.0883	< -0.0012	< 0.717	< -0.0327
γ_0	2.089 ± 0.098	2.036 ± 0.077	1.94 ± 0.13	2.054 ± 0.064
γ_1	-0.07 ± 0.37	-0.17 ± 0.31	$-0.19^{+0.35}_{-0.61}$	-0.20 ± 0.26

Table 2. Results from the power-law spherical model: the best-fitted values of Ω_k , γ_0 and γ_1 with 68% confidence level for different samples.

quantify the corresponding quantities of relatively high-mass galaxies, are very close to the estimates obtained for low-mass and intermediate-mass elliptical galaxies. Therefore, our analysis indicates the mass distribution in massive lensing galaxies can be effectively described by the power-law spherical model. Moreover, one can clearly see from Table 2 that in the framework of power-law spherical lens model, all of the three sub-samples of galaxies will provide fitting results in one direction. The most stringent constraint on Ω_k is provided by the full sample, i.e., a closed universe is strongly supported by the current observational SGL data.

3.3 Extended power-law lens model

In Fig. 5, we show the 2-D distributions with corresponding 1σ and 2σ contours for the Ω_k and lens model parameters in the case where luminosity and total mass follow different power-law distributions. Table 3 lists the best-fitted values of the parameters with 68% confidence level for different sub-samples. From the fitted range of α and δ parameters, one can notice that the luminosity density profile of elliptical galaxies is different from the total mass density profile ($\alpha \neq \delta$). Therefore, the issue of mass density profile in the early-type galaxies is still a critical one that needs to be investigated further (Cao et al. 2016). In the framework of extended power-law lens model, one could obtain a constraint on the curvature $\Omega_k < 0.0858$ at 68% C.L. from the full sample. Therefore, a universe with zero curvature (spatially flat geometry) is strongly supported by the available observations. This is the most unambiguous result of the current data set.

Concerning the sub-samples, we find that the best-fitting values of Ω_k obtained with massive galaxies are significantly different from the corresponding results with low-mass and intermediate-mass elliptical galaxies (which agree very well with the spatial flatness of the Universe). More specifically, the high-mass sub-sample did not give an upper bound on Ω_k as usual, but a lower bound at 1σ confidence level. However, a zero value of Ω_k is still included in 2σ confidence level. On the other hand, there also exists a tension between the values of lens model parameters obtained from different sub-samples (even beyond the 2σ confidence interval in α - δ plane), which supports the scheme of treating separately sub-samples with different velocity dispersion. Such conclusion has been first noticed and discussed in Cao et al. (2016). Moreover, high-mass lenses provide clearly different constraints on the slope parameters (α , δ) compared to their low-mass counterparts. Such findings can be interpreted as neither of the dark matter and stellar components is well approximated by an isothermal profile, although they seem

to work well together in building a nearly isothermal total density profile (Treu 2010). More specifically, this tendency can also be understood as the result of different dark matter density profiles, which could fall off more steeply than the stellar mass in the inner region of high-mass lensing galaxies. Our results are in perfect agreement with the recent analysis of massive early-type galaxies from large cosmological hydrodynamical simulations, which indicated that the dark matter and total density profiles tend to become slightly steeper at low redshifts, while the stellar one does not vary significantly (Peirani et al. 2018).

4 MONTE CARLO SIMULATED MOCK SAMPLE OF SGL AND QSO SYSTEMS

The ongoing and future massive surveys like LSST or DES will provide us the opportunity to discover up to three orders of magnitude more galactic-scale strong lenses that are currently known. For instance, according to the prediction of Collett (2015), the forthcoming Large Synoptic Survey Telescope (LSST) survey may potentially discover 120000 lenses for the most optimistic scenario. Therefore, we can ask the question: how precise can one determine the cosmic curvature with such a significant increase of the number of strong lensing systems? On the other hand, the uncertainty of the angular size of compact structure in radio quasars will be significantly reduced by both current and future VLBI surveys based on better uv-coverage (Pushkarev & Kovalev 2015). Consequently, one can expect to have a better distance information from the ILQSO standard ruler approach with future VLBI data.

For the purpose of our simulation we have chosen a fiducial cosmological model, which was the flat ($\Omega_k = 0$) Λ CDM with $\Omega_m = 0.30$ and $H_0 = 70$ km/s/Mpc. For the quasar data to be observed by future VLBI surveys, the mock “ θ - z ” data is generated with fixed linear size of ILQSOs equal to $l_m = 11.03$ pc. We have simulated 500 intermediate-luminosity quasars in the redshift range $0.50 < z < 6.00$, for which the fractional uncertainty of the angular size “ θ ” was taken at a level of 3%. The redshift distribution of the sources observed follows the luminosity function obtained from a combination of SDSS and 2dF (2SLAQ) surveys, the bright and faint-end slopes of which agree very well with those in the bolometric luminosity function. See Cao et al. (2017b) for more details of the specific procedure of QSO simulation.

For the strong lensing data, we use the realistic simulation of 120000 events with elliptical galaxies acting as lenses in the forthcoming LSST survey (Collett 2015). The simulation codes are available on the github.com/tcollett/LensPop.

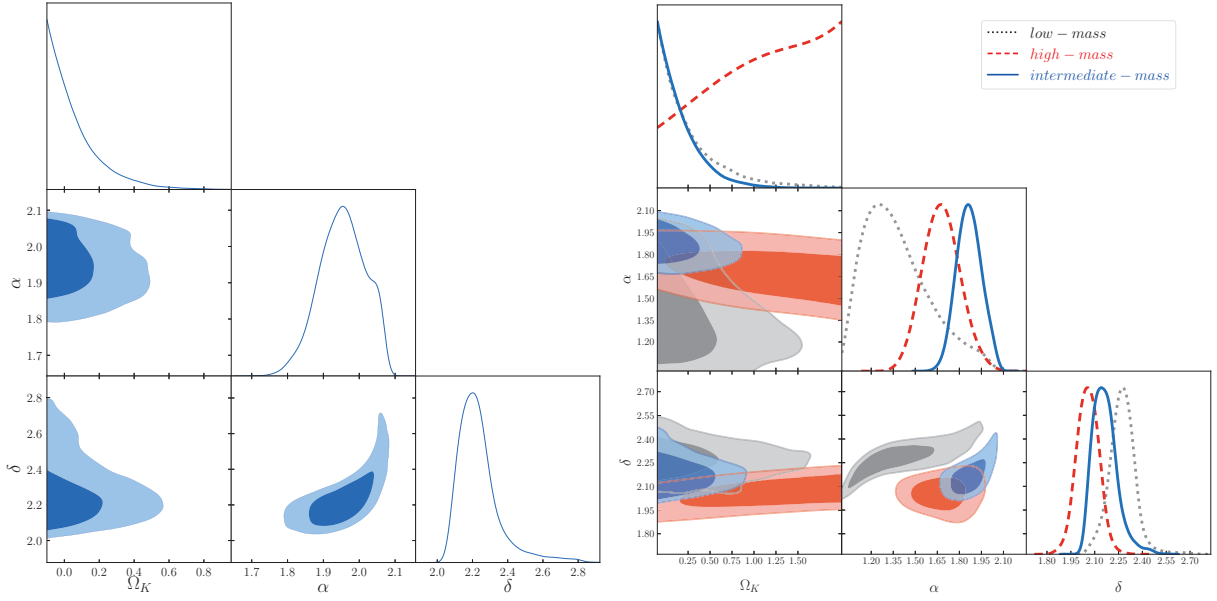


Figure 5. 2-D distributions of cosmic curvature Ω_k and SGL parameters (α , δ) constrained from the 106 SGL sample in the case of generalized lens model where stellar and total mass components follow different power-laws. 1σ and 2σ uncertainty contours are shown together with 1-D distributions of respective parameters marginalized over the remaining ones. Right: The results obtained from three sub-samples of SGL systems selected according to their velocity dispersions.

	low-mass	intermediate-mass	high-mass	full sample
Ω_k	< 0.324	< 0.22	> 0.790	< 0.0858
α	$1.38^{+0.12}_{-0.29}$	1.866 ± 0.086	1.68 ± 0.13	$1.96^{+0.086}_{-0.06}$
δ	2.274 ± 0.086	$2.164^{+0.055}_{-0.089}$	2.06 ± 0.071	$2.27^{+0.035}_{-0.16}$

Table 3. Results from the extended power-law model: the best-fitted values of Ω_k , α and δ with 68% confidence level for different samples.

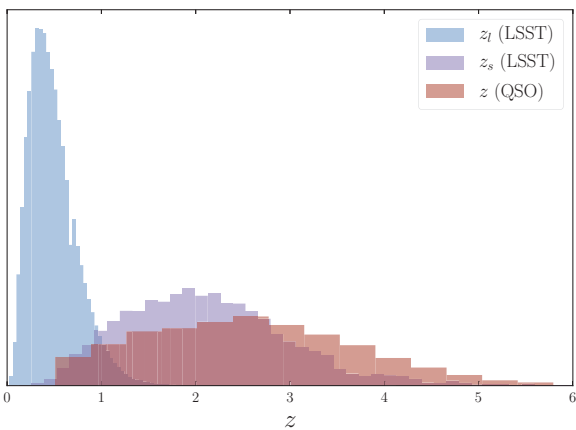


Figure 6. Redshift distribution of the simulated SGL and QSO sample.

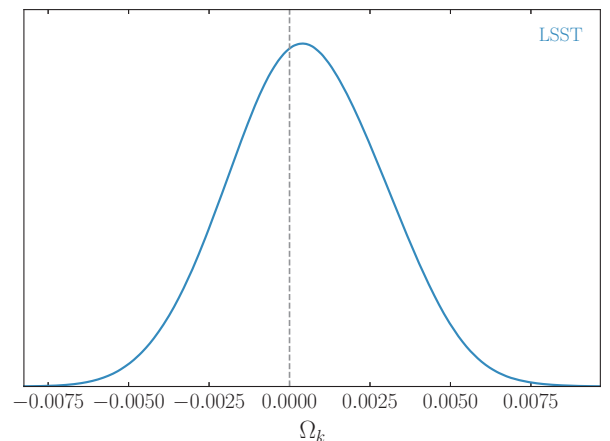


Figure 7. Constraints on the cosmic curvature achievable in the future surveys. Forecast based on simulated strong lensing and quasar data.

Considering the recent result that only the medium-mass elliptical galaxies are consistent with the singular isothermal sphere case within 1σ uncertainty (Cao et al. 2016), we restrict the velocity dispersions of lensing galaxies to the

intermediate range: $200 \text{ km/s} < \sigma_{ap} < 300 \text{ km/s}$ and obtain 16000 strong lensing systems meeting the redshift criterion $0.5 < z_l < z_s < 6.0$ in compliance with QSO data

used in parallel. In deriving the distances d_l and d_s from QSOs, we use the selection criterion $|z_{SGL} - z_{QSO}| \leq 0.005$. Fig. 6 shows the redshift coverage of the simulated QSO and SGL sample. Following the analysis of Cao et al. (2016), the fractional uncertainty of the Einstein radius and the observed velocity dispersion are respectively taken at the level of 1% and 10%. The posterior probability density for Ω_k is shown in Fig. 7. It should be emphasized that the central value of this fit reflects the fiducial model assumed i.e. flat Λ CDM. It would of course be different for a different choice of a fiducial model. However, the point is how precisely can future observational data determine the cosmic curvature and this is not so much dependent on the cosmological model used in simulations of mock catalog. We find that with about 16000 strong lensing events combined with the distance information provided by 500 compact radio quasars, one can constrain the cosmic curvature with an accuracy of $\Delta\Omega_k \simeq 10^{-3}$, which is comparable to the precision of *Planck* 2015 results.

5 CONCLUSIONS

The distance sum rule method applied to strong lensing systems is becoming an important astrophysical tool for probing the curvature of the universe without assuming any fiducial cosmological model. In this paper, attempting to alleviate the shortcomings of using SN Ia as distance indicators in the sum rule, we turned to the VLBI observations of milliarcsecond compact structure in intermediate-luminosity quasars covering the redshift range $0.46 < z < 2.76$, which have recently been demonstrated to be standardizable rulers. Providing a better redshift coverage of SGL systems they were used for distance inferences without pre-assuming any particular parameterized cosmological model. Moreover, in order to better assess the effect of lens model on measuring the cosmic curvature, we used three lens models: i) SIS model ii) spherically symmetric power-law mass profile allowing for its evolution with redshift, or iii) total and luminous mass of the lens following different power-law profiles. We show that the assumed lens model has a considerable impact on the cosmic curvature constraint found to be compatible or marginally compatible with the flat case (depending on the lens model adopted).

Furthermore, we have also divided the SGL sample into three sub-samples based on lens velocity dispersion: $\sigma_{ap} \leq 200 \text{ km s}^{-1}$ (low-mass galaxies), $200 \text{ km s}^{-1} < \sigma_{ap} \leq 300 \text{ km s}^{-1}$ (intermediate-mass galaxies) and $\sigma_{ap} > 300 \text{ km s}^{-1}$ (high-mass galaxies), and studied the effect on the measurement of curvature caused by such division. These three lens sub-samples respectively cover the redshift range of $0.075 \leq z_l \leq 0.682$, $0.082 \leq z_l \leq 0.938$, and $0.164 \leq z_l \leq 1.004$. Analysis of low, intermediate and high-mass sub-samples demonstrated that their best fitted power-law profiles of lens mass density distribution differ between them. However, they are still consistent with each other within the uncertainty limits. Discrepancies regarding the cosmic curvature are less pronounced in this case. One should bear in mind that it may not be reasonable to characterize all lenses with a uniform model. More interestingly, we find the SIS model ($f_E = 1$) is well consistent with results obtained in both low-mass and intermediate-mass (low and

intermediate velocity dispersion) galaxies. Moreover, in the framework of spherically symmetric power-law mass model, the ranges of slope parameters (γ_0, γ_1) for relatively high-mass galaxies are very close to the estimates obtained for low-mass and intermediate-mass elliptical galaxies. Therefore, our analysis indicates the mass distribution in high-mass lensing galaxies can be effectively described by the power-law spherical model. More importantly, all of the full sample and three sub-samples of galaxies, in the framework of power-law spherical lens model will provide consistent fitting results, i.e., a closed universe is favored by the current observational SGL data. Finally, when allowing the luminosity profile to be different from the total mass density profile, high-mass lenses provide clearly different constraints on the slope parameters (α, δ) compared to their low-mass counterparts. Such finding in the extended power-law lens model, which reveals the possible differences in mass density distributions of dark matter and luminous baryons in massive early-type galaxies, could help us improve our understanding of the baryonic and dark matter physics at kpc scale.

Given the limitations of the current sample, we have also performed a detailed quantitative assessment of what kind of strong lensing and quasar data are necessary to provide the constraint on cosmic curvature competitive with the CMBR data. On the one hand, ongoing and future massive surveys like the LSST will provide up to three orders of magnitude more galactic-scale strong lenses that are currently known. On the other hand, the fractional uncertainty of the angular size of the compact structure in radio quasars will be significantly reduced by both current and future radio astronomical surveys. Based on the mock catalogs of strong gravitational lenses and quasars with the current measurement accuracy, we find that the forthcoming LSST survey supplemented with the much richer data regarding ILQSO would be able to constrain cosmic curvature with the precision comparable to current CMBR data. This encourages us to consider the possibility of testing the cosmic curvature at the much higher accuracy with future surveys of strong lensing systems and high-quality radio astronomical observations of quasars.

ACKNOWLEDGMENTS

We would like to thank Zheng-Xiang Li and Jun-Qing Xia for their helpful discussions. This work was supported by National Key R&D Program of China No. 2017YFA0402600; the Ministry of Science and Technology National Basic Science Program (Project 973) under Grants No. 2014CB845806; the National Natural Science Foundation of China under Grants Nos. 11503001, 11373014, and 11690023; Beijing Talents Fund of Organization Department of Beijing Municipal Committee of the CPC; the Fundamental Research Funds for the Central Universities and Scientific Research Foundation of Beijing Normal University; and the Opening Project of Key Laboratory of Computational Astrophysics, National Astronomical Observatories, Chinese Academy of Sciences. J.-Z. Qi was supported by the China Postdoctoral Science Foundation (Grant No. 2017M620661). M. Biesiada was supported by the Foreign Talent Introduc-

tion Project and the Special Fund Supporting Introduction of Foreign Knowledge Project in China.

REFERENCES

- Ade P. A. R., et al., 2016, *Astronomy and Astrophysics*, 594, A16
- Biesiada M., Piórkowska A., Malec B., 2010, *Monthly Notices of the Royal Astronomical Society*, 406, 1055
- Biesiada M., Malec B., Piórkowska A., 2011, *Research in Astronomy and Astrophysics*, 11, 641
- Bolejko K., 2017a, arXiv preprint arXiv:1707.01800
- Bolejko K., 2017b, *Classical and Quantum Gravity*, 35, 024003
- Bolton A. S., et al., 2012, *The Astrophysical Journal*, 757, 82
- Bonamente M., Joy M. K., LaRoque S. J., Carlstrom J. E., Reese E. D., Dawson K. S., 2006, *The Astrophysical Journal*, 647, 25
- Cai R., Guo Z., Yang T., 2016, *Physical Review D*, 93, 043517
- Cao S., Liang N., 2011, *Research in Astronomy and Astrophysics*, 11, 1199
- Cao S., Zhu Z., 2011, *Science China-physics Mechanics & Astronomy*, 54, 2260
- Cao S., Zhu Z.-H., 2012, *A&A*, 538, A43
- Cao S., Zhu Z.-H., 2014, *Physical Review D*, 90, 083006
- Cao S., Pan Y., Biesiada M., Godlowski W., Zhu Z.-H., 2012, *Journal of Cosmology and Astroparticle Physics*, 03, 016
- Cao S., Biesiada M., Zheng X., Zhu Z.-H., 2015a, *The Astrophysical Journal*, 806, 66
- Cao S., Biesiada M., Gavazzi R., Piórkowska A., Zhu Z.-H., 2015b, *The Astrophysical Journal*, 806, 185
- Cao S., Biesiada M., Yao M., Zhu Z., 2016, *Monthly Notices of the Royal Astronomical Society*, 461, 2192
- Cao S., Biesiada M., Jackson J., Zheng X., Zhao Y., Zhu Z.-H., 2017a, *Journal of Cosmology and Astroparticle Physics*, 02, 012
- Cao S., Zheng X., Biesiada M., Qi J., Chen Y., Zhu Z.-H., 2017b, *A&A*, 606, A15
- Cao S., Biesiada M., Qi J., Pan Y., Zheng X., Xu T., Ji X., Zhu Z.-H., 2018, *Eur. Phys. J. C*, 78, 749
- Chen G., Ratra B., 2003, *The Astrophysical Journal*, 582, 586
- Clarkson C., Bassett B., Lu T. H.-C., 2008, *Physical Review Letters*, 101, 011301
- Collett T. E., 2015, *The Astrophysical Journal*, 811, 20
- Denissenya M., Linder E. V., Shafieloo A., 2018, *Journal of Cosmology and Astroparticle Physics*, 03, 041
- Foreman-Mackey D., Hogg D. W., Lang D., Goodman J., 2013, *Publications of the Astronomical Society of the Pacific*, 125, 306
- Grillo C., Lombardi M., Bertin G., 2008, *Astronomy and Astrophysics*, 477, 397
- Gurvits L. I., 1994, *The Astrophysical Journal*, 425, 442
- Gurvits L., Kellermann K., Frey S., 1998, arXiv preprint astro-ph/9812018
- Holanda R., Lima J., Ribeiro M., 2011, *Astronomy & Astrophysics*, 528, L14
- Jackson J., Dodgson M., 1997, *Monthly Notices of the Royal Astronomical Society*, 285, 806
- Jimenez R., Loeb A., 2002, *ApJ*, 573, 37
- Kellermann K., 1993, *Nature*, 361, 134
- Koopmans L. V. E., Treu T., Bolton A. S., Burles S., Moustakas L. A., 2006, *The Astrophysical Journal*, 649, 599
- Li X., Cao S., Zheng X., Li S., Biesiada M., 2016a, *Research in Astronomy and Astrophysics*, 16, 84
- Li Z., Gonzalez J., Yu H., Zhu Z.-H., Alcaniz J., 2016b, *Physical Review D*, 93, 043014
- Li Z., Wang G.-J., Liao K., Zhu Z.-H., 2016c, *The Astrophysical Journal*, 833, 240
- Li X., Cao S., Zheng X., Qi J., Biesiada M., Zhu Z.-H., 2017, *Eur. Phys. J. C*, 77, 677
- Liao K., Li Z., Wang G.-J., Fan X.-L., 2017, *The Astrophysical Journal*, 839, 70
- Lima J., Alcaniz J., 2002, *The Astrophysical Journal*, 566, 15
- Ma Y., Zhang J., Cao S., Zheng X., Xu T., Qi J., 2017, *Eur. Phys. J. C*, 77, 891
- Moresco M., et al., 2012, *JCAP*, 1208, 006
- Ofek E. O., Rix H.-W., Maoz D., 2003, *Monthly Notices of the Royal Astronomical Society*, 343, 639
- Ooba J., Ratra B., Sugiyama N., 2018, *The Astrophysical Journal*, 864, 80
- Peirani S., et al., 2018, arXiv: Astrophysics of Galaxies
- Percival W. J., et al., 2010, *Monthly Notices of the Royal Astronomical Society*, 401, 2148
- Pushkarev A. B., Kovalev Y. Y., 2015, *Monthly Notices of the Royal Astronomical Society*, 452, 4274
- Qi J.-Z., Zhang M.-J., Liu W.-B., 2016, arXiv preprint arXiv:1606.00168
- Qi J.-Z., Cao S., Biesiada M., Zheng X., Zhu Z.-H., 2017, *Eur. Phys. J. C*, 77, 502
- Qi J.-Z., Cao S., Biesiada M., Xu T.-P., Wu Y., Zhang S.-X., Zhu Z.-H., 2018, *Research in Astronomy and Astrophysics*, 18, 066
- Rana A., Jain D., Mahajan S., Mukherjee A., 2017, *Journal of Cosmology and Astroparticle Physics*, 03, 028
- Räsänen S., Bolejko K., Finoguenov A., 2015, *Physical review letters*, 115, 101301
- Ruff A. J., Gavazzi R., Marshall P. J., Treu T., Auger M. W., Braut F., 2011, *The Astrophysical Journal*, 727, 96
- Schwab J., Bolton A. S., Rappaport S. A., 2009, *The Astrophysical Journal*, 708, 750
- Seikel M., Clarkson C., Smith M., 2012a, *Journal of Cosmology and Astroparticle Physics*, 06, 036
- Seikel M., Yahya S., Maartens R., Clarkson C., 2012b, *Physical Review D*, 86, 083001
- Takada M., Doré O., 2015, *Physical Review D*, 92, 123518
- Treu T., 2010, *Annual Review of Astronomy and Astrophysics*, 48, 87
- Vishwakarma R., 2001, *Classical and Quantum Gravity*, 18, 1159
- Walsh D., Carswell R. F., Weymann R. J., 1979, *Nature*, 279, 381
- Wei J.-J., Wu X.-F., 2017, *The Astrophysical Journal*, 838, 160
- Xia J.-Q., Yu H., Wang G.-J., Tian S.-X., Li Z.-X., Cao S., Zhu Z.-H., 2017, *The Astrophysical Journal*, 834, 75
- Xu T., Cao S., Jing-Zhao Q., Marek B., Xiaogang Z., Zong-Hong Z., 2018, *Journal of Cosmology and Astroparticle Physics*, 06, 042
- Yang T., Guo Z.-K., Cai R.-G., 2015, *Physical Review D*, 91, 123533
- Zhang M.-J., Xia J.-Q., 2016, *Journal of Cosmology and Astroparticle Physics*, 12, 005
- Zheng X., Biesiada M., Cao S., Qi J., Zhu Z.-H., 2017, *Journal of Cosmology and Astroparticle Physics*, 2017, 030
- Zhu Z.-H., Fujimoto M.-K., 2002, *The Astrophysical Journal*, 581, 1

This paper has been typeset from a $\text{\TeX}/\text{\LaTeX}$ file prepared by the author.